Nucleic Acids Research, 1995, Vol. 23, No. 7 1215–1222

Interaction of dimeric intercalating dyes with single-stranded DNA

Hays S. Rye and Alexander N. Glazer*

Department of Molecular and Cell Biology, University of California, Berkeley, CA 94720, USA

Received November 23, 1994; Revised and Accepted February 15, 1995

ABSTRACT

The unsymmetrical cyanine dye thiazole orange homodimer (TOTO) binds to single-stranded DNA (ssDNA, M13mp18 ssDNA) to form a fluorescent complex that is stable under the standard conditions of electrophoresis. The stability of this complex is indistinguishable from that of the corresponding complex of TOTO with double-stranded DNA (dsDNA). To examine if TOTO exhibits any binding preference for dsDNA or ssDNA, transfer of TOTO from pre-labeled complexes to excess unlabeled DNA was assayed by gel electrophoresis. Transfer of TOTO from M13 ssDNA to unlabeled dsDNA proceeds to the same extent as that from M13 dsDNA to unlabeled dsDNA. A substantial amount of the dye is retained by both the M13 ssDNA and M13 dsDNA even when the competing dsDNA is present at a 600-fold weight excess; for both dsDNA and ssDNA, the pre-labeled complex retains approximately one TOTO per 30 bp (dsDNA) or bases (ssDNA). Rapid transfer of dye from both dsDNA and ssDNA complexes is seen at Na^+ concentrations >50 mM. Interestingly, at higher Na^+ or Mg^{2+} concentrations, the M13 ssDNA–TOTO complex appears to be more stable to intrinsic dissociation (dissociation in the absence of competing DNA) than the complex between TOTO and M13 dsDNA. Similar results were obtained with the structurally unrelated dye ethidium homodimer. The dsDNA– and ssDNA–TOTO complexes were further examined by absorption, fluorescence and circular dichroism spectroscopy. The surprising conclusion is that polycationic dyes, such as TOTO and EthD, capable of bis-intercalation, interact with dsDNA and ssDNA with very similar high affinity.

INTRODUCTION

In a series of recent studies, we have shown that various fluorescent polycationic homodimeric and heterodimeric dyes form complexes with double-stranded DNA (dsDNA) so stable that they could be separated by gel electrophoresis and detected with very high sensitivity in the absence of free dye (1). We have exploited such complexes for the detection and sizing of dsDNA restriction fragments in agarose gels and in capillary electrophoresis (2–5), to examine the properties of dsDNA binding proteins using the gel mobility shift assay (6) and to detect and quantitate nucleic acids in solution (7). Others have used these dimeric dyes for fluorescence detection and sizing of individual DNA fragments (8,9), for the ultra-high sensitivity detection of dsDNA in flow cytometry (10), for the analysis of PCR products (11) and for the examination of the static and dynamic properties of isolated DNA molecules (12–14).

However, little is known about the binding specificity of these dimeric dyes for different nucleic acid structures. We have shown that both single-stranded DNA (ssDNA) and RNA can be detected in solution with high sensitivity by exploiting the fluorescence of their complexes with dimeric unsymmetrical cyanine dyes (7). While this result implies binding of these dyes to nucleic acid structures other than canonical dsDNA, the nature of this interaction and the relative affinities of the dyes for various nucleic acid targets is unknown.

This study compares the interaction of two structurally different polycationic dimeric dyes, thiazole orange homodimer [TOTO; (4)] and ethidium homodimer [EthD; (15–18)] with single- and double-stranded DNAs under a variety of conditions. The question of finding conditions which might allow selective labeling of dsDNA in the presence of ssDNA and vice versa is briefly addressed. The answer to this question is a prerequisite to the potential application of these dyes to *in situ* hybridization and novel fluorescent probe design (1). In light of recent studies employing TOTO as a fluorescent stain to track the intracellular migration of micro-injected plant virus RNA and DNA (19,20), an understanding of the various possible binding targets for polycationic dimeric fluorophores appears particularly pertinent.

MATERIALS AND METHODS

Preparation of dye and DNA stock solutions

Ethidium homodimer [EthD; ε = 8900/M/cm at 492 nm in water (21)] was purchased from Molecular Probes, Inc. (Eugene, OR). Thiazole orange homodimer [TOTO; ε = 131 700/M/cm at 507 nm in methanol (4)] was synthesized as previously described (4). Stock dye solutions and aqueous stock solutions for immediate use (with aqueous stock solutions always prepared freshly in 40 mM Tris–acetate, 2 mM EDTA, pH 8.2; henceforth designated

*To whom correspondence should be addressed at: MCB: Stanley/Donner ASU, 229 Stanley Hall #3206, University of California, Berkeley, CA 94720-3206, USA

'TAE' buffer) were prepared and stored as previously described (3,4).

Closed-circular single-stranded M13mp18 DNA (M13 ssDNA) was produced from M13mp18 phage utilizing the F'-plus *E.coli* strain DH5αF' (Gibco-BRL; Gaithersberg, MD), essentially as outlined in (22). Purified M13 ssDNA was linearized by first hybridizing a short (15mer) complementary oligonucleotide to the ssDNA, centered across the unique *Bam*HI cleavage site in the cloning polylinker of the M13mp18 genome. Typically, 400 μg of M13 ssDNA were mixed with slightly more than one mole equivalent (~20–30% excess) of oligonucleotide in a total volume of 230 μl which contained the *Bam*HI cleavage buffer at the appropriate concentration. This mixture was then heated at 85°C for 5 min, at 68°C for 10 min, and then allowed to cool to room temperature for 30 min. Subsequently, 400 U (in 20 μl) of *Bam*HI (New England Biolabs; Beverly, MD) was added to the mixture and the sample was incubated at 37°C for ~2 h. After digestion, the linearized M13 ssDNA was purified by electrophoresis on a 1% agarose gel in TAE buffer. The clarified M13 ssDNA band was cut out of the gel and the ssDNA was electroeluted in TAE buffer by placing the gel slice in a dialysis membrane bag (3500 MW cutoff, 18 mm wide) and eluting the DNA at 2 V/cm for 3–4 h. The field polarity was then reversed and the field strength increased to 6 V/cm for 1 min. The solution containing the linear M13 ssDNA was removed from the dialysis bag and the bag was rinsed once with a small amount of buffer. The ssDNA from the combined fractions was then precipitated with sodium acetate–ethanol and reconstituted in a small volume of 10 mM Tris–HCl–1 mM EDTA, pH 8.0. This procedure typically gave yields of ~60%.

Both M13mp18 RF and pBluescript (Stratagene; La Jolla, CA) were produced essentially as described in (22), and were first purified using a Qiagen (Chatsworth, CA) column followed by CsCl/ethidium bromide equilibrium centrifugation. The double stranded plasmids (~100 μg) were each cut at a single site with *Bam*HI (80–100 U). The linear dsDNA was then extracted with phenol–chloroform and recovered by precipitation with sodium acetate–ethanol. Analysis by agarose gel electrophoresis showed nearly complete single cutting of the plasmids. Calf thymus DNA (Sigma; St Louis, MO; Type I) was first sheared by repeated passage through a small gauge needle and then purified by phenol–chloroform extraction and sodium acetate–ethanol precipitation. Stock solutions of dsDNA samples were stored at –20°C, while M13 ssDNA samples were stored at 4°C.

Absorption, circular dichroism and fluorescence spectroscopy

Absorption spectra were acquired on a computer-controlled dual-beam Perkin-Elmer (Norwalk, CN) λ6 UV/Vis Spectrophotometer using a 1 cm path length quartz cuvette. Circular dichroism (CD) spectra were measured with a computer-controlled Aviv 62DS Circular Dichroism Spectrometer with a 1 cm path length, black-walled quartz cuvette. Fluorescence measurements were performed in 4 mm square quartz cells with a Perkin-Elmer MPF44B spectrofluorimeter fitted with a high sensitivity cell holder assembly equipped with concave mirrors (Perkin-Elmer part no. 0010-0500) and connected to a Perkin-Elmer Hitachi 057 plotter.

Dye–DNA complex formation and agarose gel electrophoresis

The following general protocol was used for the formation of all DNA–dye complexes intended for gel analysis, taking care to observe mixing order and concentration limits as outlined previously (3,4,23). All operations were performed at room temperature. The DNA and dye solutions were individually diluted into TAE buffer prior to use. For experiments under a single set of conditions, mixing was performed in a total volume of 37.5 μl in sterile plastic Eppendorf tubes. The DNA–dye solutions were well mixed by re-pipeting and the samples incubated for a minimum of 30 min in the dark. For competition, ionic strength and cation dependence experiments, different DNA samples were initially labeled separately with either TOTO or EthD in TAE as described above, but in a volume of ~550 μl. Following initial incubation, different amounts of either unlabeled DNA, buffer or 5 M NaCl were mixed with aliquots (15.3 μl) of the solution of pre-labeled DNA to achieve the desired ionic strength or excess of unlabeled DNA over dye–DNA complex in a final volume of 37.5 μl. The samples were then incubated in the dark for an additional 30–45 min. Ficoll [Sigma; type 400; 25% (w/v) in TAE] was mixed with all sample solutions to a final concentration of 6.25% (12.5 μl addition to 37.5 μl mix). For all experiments, 10 μl samples of these mixtures were then immediately loaded onto an agarose gel (typically 1%, w/v). Agarose (ultrapure; Gibco-BRL) was cast in a vertical format as previously described (3). All gels were made in TAE and electrophoresis was conducted in the same buffer. Gels were pre-run for 1–2 h at 10 V/cm and then run for 1 h at 10 V/cm after sample application.

For off-rate experiments, DNA samples were mixed with TOTO in TAE buffer at the desired labeling ratio in a volume of 550 μl and incubated at room temperature in the dark for 1–2 h. Subsequently, 76.5 μl of this mixture was mixed with TAE buffer and Ficoll in a total volume of 250 μl to give a final Ficoll concentration of 6.25%, and the sample was then placed on ice in the dark. Aliquots (10 μl) of this final mix were then loaded onto the gel at 12 min intervals. Electrophoresis was conducted at 10 V/cm.

Fluorescence detection in gels and image analysis

After electrophoresis, gels were scanned with a two-color, confocal fluorescence gel imaging system as previously described (24,25). The fluorescence of the TOTO–DNA samples was collected from 500–565 nm and the EthD fluorescence was collected from 610–700 nm. The resulting unprocessed binary data files (16-bits/pixel) were imported into 8-bit Macintosh TIFF files. The resulting images were processed with the NIH image processing program Image 1.44 and IPLab (Signal Analytics Corp.; Vienna, VA). Fluorescence intensity values of the detected bands were calculated by integration with the program Scan Analysis (BioSoft; Cambridge, UK). For the purposes of display, the gel images were contrast-enhanced with IPLab by applying a non-linear function, calculated based upon the histogram of the intensity distribution for the visible bands, to the file look-up table (8-bit gray). The result of this transform, as applied to a linear 8-bit gray scale, is displayed with each gel image.

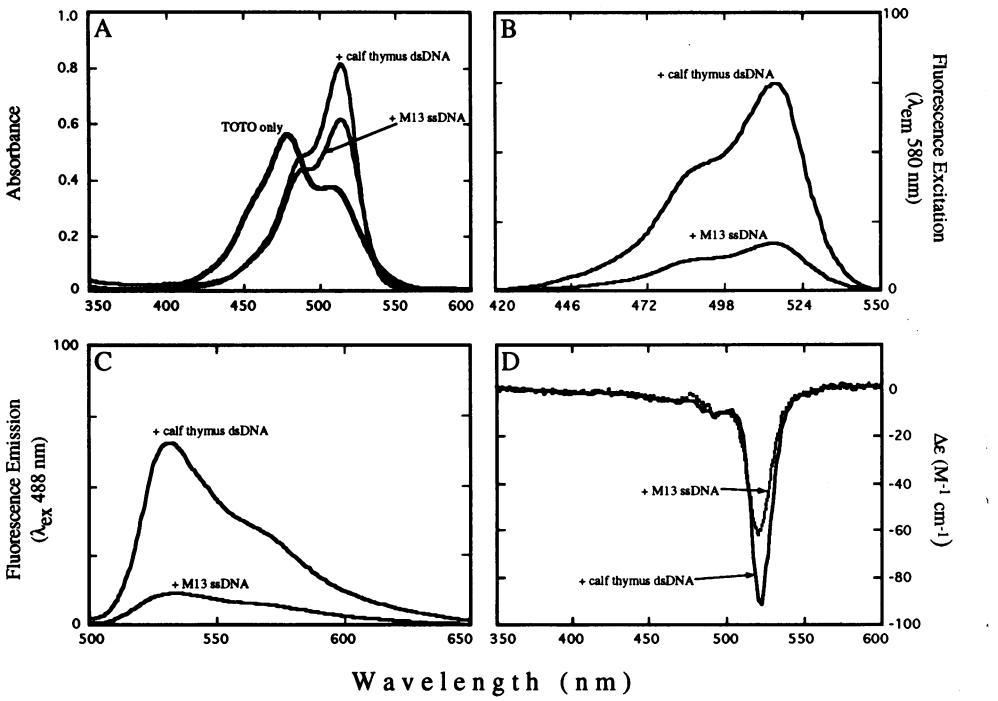

Figure 1. Absorption (**A**), fluorescence excitation (**B**) and emission (**C**) and induced circular dichroism (**D**) spectra of dsDNA– and ssDNA–TOTO complexes. Panel A shows the absorption spectra of unbound TOTO and the dye bound to calf thymus dsDNA and M13 ssDNA. In each case, TOTO (final concentration 7.6×10^{-6} M) was mixed with DNA at 15 bp/dye (dsDNAs) or 15 bases/dye (ssDNA). Panels B and C show the fluorescence excitation and emission spectra, respectively, of TOTO complexes with M13 ssDNA and calf thymus dsDNA. In each case, TOTO (final concentration 1.1×10^{-7} M) was mixed with the DNAs at 15 bp/dye or 15 bases/dye (for ssDNA). For excitation spectra, the emission wavelength was set at 580 nm, and for emission spectra, the excitation wavelength was set at 488 nm. The excitation and emission slit widths were set at 6 nm for all spectra. All fluorescence spectra have been normalized for differences in the absorption of the various complexes at the excitation wavelength. Panel D shows the induced circular dichroism (CD) spectra of M13 ssDNA–TOTO and calf thymus dsDNA–TOTO complexes. The samples are identical to those shown in panel A. All DNA solutions were in TAE buffer containing 100 mM NaCl.

RESULTS

Spectroscopic characteristics of dsDNA– and ssDNA–TOTO complexes

Absorption spectroscopy. Binding of TOTO to various single- and double-stranded DNAs led in all cases to large changes in the absorption spectrum of the dye. Free TOTO shows a strong absorption peak at 480 nm and a somewhat weaker absorption band at 512 nm (Fig. 1A). Binding of TOTO to dsDNAs at a dye/bp ratio of 1:15 led in all cases to a red shift of the 480 nm band with a marked decrease in its oscillator strength and a small red shift of the 512 nm band (to ~515 nm) together with large increase in its oscillator strength (Fig. 1A). Surprisingly, binding of TOTO to M13 ssDNA led to the same qualitative changes in the spectrum of the dye, except that the increase in the oscillator strength of the 515 nm absorption band was about two-thirds that seen with calf thymus dsDNA (Fig. 1).

Fluorescence spectroscopy. The shapes of the fluorescence excitation and emission spectra of TOTO in the presence of M13 ssDNA (Fig. 1B and C) are very similar to those of TOTO–calf thymus dsDNA complexes. The emission maxima are at 532 nm for TOTO–dsDNA and 535 nm for TOTO–M13 ssDNA. However, at 15 bases/dye the TOTO–M13 ssDNA complex is ~5-fold less fluorescent than the complex with calf thymus dsDNA at 15 bp/dye. In addition, the TOTO–M13 ssDNA emission spectrum is broader than the corresponding emission from TOTO–dsDNA, and the ratio of the 532 nm peak to the shoulder at 570 nm decreases from ~2.0 for the TOTO–dsDNA complex to 1.5 for the TOTO–M13 ssDNA complex.

Titration of ssDNA and dsDNA with TOTO: effect of site occupancy on fluorescence intensity. Fluorescence data obtained on titration of M13 dsDNA and M13 ssDNA with identical amounts of TOTO at ratios ranging from 123:1 to 12:1 base pairs/dye (dsDNA) or bases/dye (ssDNA) are shown in Figure 2A. For both DNAs, a fluorescence plateau is reached at 4–5 bp or bases/dye, with an intensity 2–3-fold greater for the M13 dsDNA than for the ssDNA.

Titration of a fixed amount of TOTO with either M13 dsDNA or ssDNA showed that the fluorescence emission per bound dye reaches a maximum for dsDNA at ~30–40 bp/dye and for ssDNA at ~40–50 bases/dye. The fluorescence intensity of TOTO molecules bound to M13 ssDNA at ratios <1:50 dye/bases is nearly equivalent to that of TOTO molecules bound at such ratios to M13 dsDNA (Fig. 2B). An important result is that the fluorescence emission of TOTO bound to dsDNA decreases ~2-fold with increase in the dye/DNA ratio from 1:50 dye/bp to 1:5 dye/bp. The emission of TOTO bound to ssDNA over the same range of dye/DNA ratios decreases ~5-fold.

Circular dichroism spectroscopy. The induced CD spectra of TOTO in the presence of calf thymus dsDNA and M13 ssDNA are shown in Figure 1D. Free TOTO has only a very weak negative CD in aqueous buffer ($\Delta\varepsilon \cong -8$/M/cm; $\lambda_{max} = 475$ nm). This weak intrinsic CD appears to originate from the thiazole orange head group alone, since free thiazole orange monomer

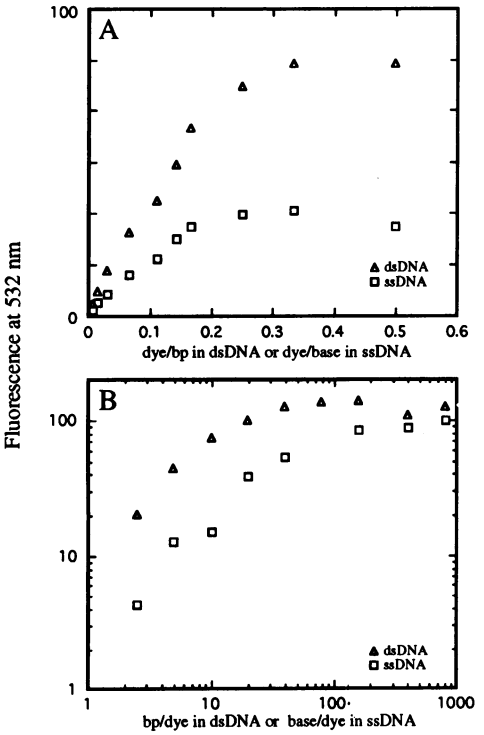

Figure 2. Fluorescence titration of M13 dsDNA (Δ) and ssDNA (□) in TAE buffer with TOTO. (**A**) Shows a titration of a fixed concentration of either dsDNA or ssDNA with TOTO. The DNA concentration was 1.6×10^{-7} M bp (M13 dsDNA) or bases (M13 ssDNA) and the TOTO concentration was adjusted from 1.3×10^{-9} to 7.8×10^{-8} M. Each data point represents the fluorescence of the sample at 532 nm corrected for a slight dilution due to the titration with dye. (**B**) Shows a titration of a fixed concentration of TOTO with increasing amounts of either dsDNA or ssDNA in TAE buffer. In this case, the TOTO concentration was held constant by preparing a series of reaction mixtures in which the TOTO concentration was 3.1×10^{-9} M and the DNA concentration was varied from 7.9×10^{-9} M bp (M13 dsDNA) or bases (M13 ssDNA) to 3.1×10^{-6} M bp or bases. Each data point represents the fluorescence of the sample at 532 nm. For all data, the excitation wavelength was set at 488 nm and the emission was collected from 460 to 650 nm with slit widths set at 8 nm for panel A and 10 nm for panel B.

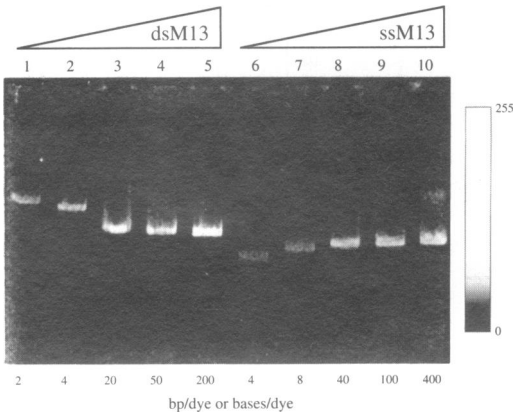

Figure 3. Effect of site occupancy on the electrophoretic mobility and fluorescence intensity of M13 dsDNA–TOTO and ssDNA–TOTO complexes. For all lanes, a constant amount of TOTO (final concentration 1.6×10^{-8} M) was mixed with different amounts of either linear M13 dsDNA (lanes 1–5) or linear M13 ssDNA (lanes 6–10) at the DNA to dye ratios indicated below the figure, where bp/dye and bases/dye refer to dsDNA–TOTO complexes and ssDNA–TOTO complexes, respectively. The total load of DNA was as follows: lanes 1 and 6: 200 pg; lanes 2 and 7: 400 pg; lanes 3 and 8: 2 ng; lanes 4 and 9: 5 ng; lanes 5 and 10: 20 ng. All mixing was conducted in TAE buffer and samples were incubated at room temperature for 30 min prior to gel loading and electrophoresis. The gel image shown was acquired by a confocal fluorescence scan of a vertical agarose gel and the color table to the right of the figure is an 8-bit gray scale that has been subjected to the same contrast enhancement as the gel image data (see Materials and Methods).

shows a similar CD spectrum, though the monomer spectrum has a different maximum wavelength (λ_{max} = 507 nm; data not shown). The induced CD spectra of TOTO bound to dsDNA and ssDNA are strikingly similar, both showing a prominent negative CD peak centered around 520 nm, differing only in magnitude when a fixed amount of dye is bound to either DNA at 15:1 bp or bases per dye. When a fixed amount of TOTO is titrated with dsDNA, the shape of this CD spectrum did not vary with the DNA/dye ratio over the range 40:1 to 5:1 bp/dye. The magnitude of the induced CD observed with dsDNA decreased ~10% when the DNA/dye ratio was decreased from 40:1 to 15:1 bp/dye but did not change further at lower DNA/dye ratios (26). The shape of the induced CD seen with M13 ssDNA also did not change from 40:1 to 15:1 bases/dye and the magnitude decreased only 10%. However, at 5:1 bases/dye, the M13 ssDNA–TOTO CD spectrum became considerably more complex, with the prominent negative peak at 520 nm decreasing significantly, a new negative peak appearing at ~450 nm and a positive peak appearing at ~475 nm (26).

Stability of TOTO–M13 ssDNA complexes to electrophoresis

The fluorescence titration studies shown in Figure 2 indicated that TOTO shows a similar affinity for M13 ssDNA and dsDNA. This conclusion is directly testable by comparing the stabilities of these TOTO–DNA complexes to electrophoresis.

Our previous studies established that TOTO–dsDNA complexes dissociate very slowly under the standard conditions of gel electrophoresis [$t_{0.5}$ = 660 min; (2)]. The experiment shown in Figure 3 compares the behavior and stability of TOTO complexes with M13 dsDNA (lanes 1–5) and M13 ssDNA (lanes 6–10) at various dye/DNA ratios. The stability of the complexes with ssDNA is similar to those with dsDNA. In fact, the rates of dissociation of TOTO–ssDNA and TOTO–dsDNA complexes were indistinguishable within experimental error (26).

The two types of complexes do show distinctive electrophoretic properties. As the dye/DNA ratio increases, the electrophoretic mobility of both types of dye–DNA complexes is altered, but in opposite directions. As the saturation of the DNAs with TOTO increases, the mobility of the M13 dsDNA decreases, whereas that of M13 ssDNA increases (see Fig. 3). Retardation of dsDNA fragments during electrophoresis, induced by the stable binding of intercalating dye molecules (polyacridines), has been previously noted and assumed to be due to charge neutralization and the conformational rigidification of the dsDNA helical structure (27). On the other hand, the increase in the mobility of M13 ssDNA on binding TOTO can be explained through the dye-induced collapse of coulombic repulsions between the phosphates of the single-stranded coil. These repulsive interactions would normally serve to extend the structure of the

single-stranded coil, and diminution of this repulsion by stable dye binding would permit partial chain collapse and therefore increased electrophoretic mobility. This interpretation is supported by early observations that the intercalators proflavine and 9-aminoacridine decrease the viscosity of denatured DNA, while they increase the viscosity of native DNA (28).

The fluorescence intensities per added dye of the bands of TOTO–DNA complexes, formed at various DNA/dye ratios shown in Figure 3, correspond to those predicted from the plot of the dependence of fluorescence intensity on the DNA/dye ratio (Fig. 2) for the titration in solution.

TOTO transfer between dsDNA and ssDNA at low Na^+ concentration. Figure 4A shows a titration of a M13 dsDNA–TOTO complex (initially formed at 15 bp/dye) with increasing amounts of unlabeled, linear pBluescript dsDNA. As reported previously (4), the competing dsDNA removes TOTO from the original complex up to a certain site occupancy. Little further removal of TOTO is seen beyond that point; even at a pBluescript dsDNA to M13 dsDNA ratio of 900:1 (w/w), a large quantity of dye remains bound to the original DNA. Figure 4B shows a similar titration of a M13 ssDNA–TOTO complex with pBluescript dsDNA. Again, large amounts of competing dsDNA remove TOTO from the preformed complex. However, as for the TOTO–M13 dsDNA complex, a substantial amount of dye remains bound to the ssDNA even in the presence of a 600-fold weight excess of competing dsDNA.

The modest decreases in the fluorescence of the TOTO–M13 dsDNA or TOTO–M13 ssDNA bands seen as dye is transferred to pBluescript dsDNA, are anticipated from the increases in TOTO fluorescence intensity (documented in Figs 2 and 3) that accompany decreases in site occupancy. As TOTO molecules are removed from the preformed M13 complexes by the pBluescript dsDNA, the remaining dye becomes more fluorescent. This phenomenon makes quantitation of the dye lost from the TOTO–M13 dsDNA or TOTO–M13 ssDNA complexes very difficult. However, the very large amounts of the added pBluescript dsDNA ensure that the dye/DNA ratio in the pBluescript dsDNA bands is such that the fluorescence intensity of these bands is independent of the dye/DNA ratio and provides a direct measure of the amount of dye transferred. By measuring the amount of dye transferred to the competing DNA in a series of experiments like that shown in Figure 4, it can be demonstrated that the amount of dye transferred from the TOTO–M13 dsDNA complex is the same within experimental error as the amount transferred from the M13 ssDNA complex (26). For both types of DNA labeled at 15:1 bp or bases per dye, excess pBluescript dsDNA removes a maximum of ~50–60% of the initially bound TOTO, and this extent of dye removal is reached at a pBluescript/M13 DNA ratio of 100:1 (w/w). The competition experiments indicate that the affinity of TOTO is similar for single-stranded and double-stranded nucleic acids.

TOTO transfer between dsDNA and ssDNA at high Na^+ concentration. The experiments shown in Figures 3 and 4 were performed at low Na^+ concentrations (in TAE buffer containing ~4 mM Na^+) where TOTO showed similar affinity for dsDNA and ssDNA. Once the [Na^+] is raised >50 mM, dye transfer from the M13 dsDNA–TOTO or M13 ssDNA–TOTO complexes to excess competing DNA is complete (data not shown). However, in the absence of competing DNA, M13 ssDNA–TOTO complexes are more resistant than M13 dsDNA–TOTO complexes to

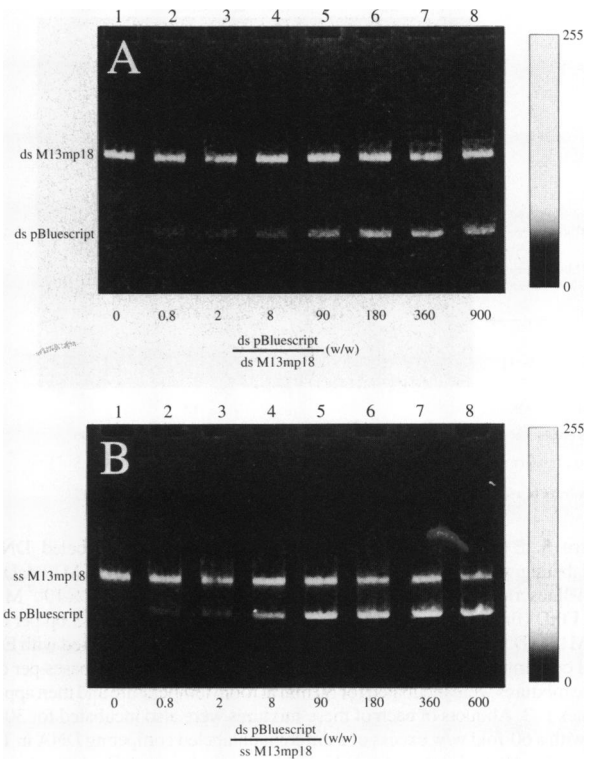

Figure 4. Transfer of TOTO from either a dsDNA complex (**A**) or a ssDNA complex (**B**) initially at 15 bp/dye (M13 dsDNA) or bases/dye (M13 ssDNA) to excess unlabeled dsDNA. All solutions were in TAE buffer. For panel A, the linear M13 dsDNA was initially labeled by mixing TOTO (final concentration 8.6×10^{-9} M) with dsDNA (final concentration 1.3×10^{-7} M bp) at a molar ratio 15:1 bp/dye. After 30 min at room temperature, aliquots of the sample were mixed with different amounts of linear pBluescript dsDNA to give the ratios (w/w) of pBluescript to M13 dsDNA indicated below the figure. These samples were incubated for an additional 30–45 min at room temperature prior to gel loading and electrophoresis. The total M13 dsDNA load for each lane was 250 pg and the pBluescript dsDNA load ranged from 200 pg to 225 ng. For panel B, the linear M13 ssDNA was initially labeled by mixing TOTO (final concentration 3.4×10^{-8} M) with ssDNA (final concentration 5.1×10^{-7} M bases) at a molar ratio of 15:1 bases/dye. The labeled ssDNA was then mixed with competing pBluescript dsDNA as described above to achieve the ratios (w/w) indicated below the figure. The total M13 ssDNA load for each lane was 500 pg and that of pBluescript dsDNA ranged from 400 pg to 300 ng. For acquisition of the gel image, see legend to Figure 3.

simple cation-induced dissociation of the dye. For example, in samples containing 500 mM NaCl, the fluorescence of the M13 dsDNA–TOTO mixture was 14% and that of the M13 ssDNA–TOTO mixture was 47% relative to the fluorescence of controls in TAE buffer containing ~4 mM Na^+. The corresponding relative fluorescence values for mixtures in 100 mM $MgCl_2$ were 4 and 25%, respectively.

Ethidium homodimer (EthD) transfer between dsDNA and ssDNA at low Na^+ ion concentration

The stability of ssDNA–EthD and dsDNA–EthD complexes to electrophoresis was compared to assess the generality of the observations with the TOTO complexes. The EthD complexes with ssDNA and dsDNA show similar stability to gel electrophoresis (Fig. 5, lanes 1–3). As seen for the TOTO complexes, the M13 ssDNA–EthD complex is also less fluorescent than the

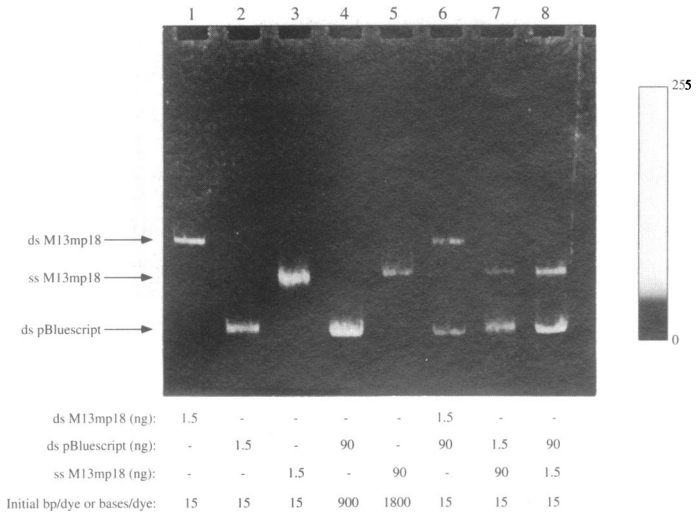

Figure 5. Extent of EthD transfer from pre-labeled to unlabeled DNAs. Pre-labeling with EthD in TAE buffer was performed as follows: M13 dsDNA and pBluescript dsDNA were each mixed (final concentration 7.7×10^{-7} M bp) with EthD (final concentration 5.2×10^{-8} M) to give a ratio of 15 bp per dye, and M13 ssDNA (final concentration 1.5×10^{-6} M bases) was mixed with EthD (final concentration 1.0×10^{-7} M) to give a labeling ratio of 15 bases per dye. These mixtures were incubated for 30 min at room temperature and then applied to lanes 1–3. Aliquots of each of these mixtures were also incubated for 30–45 min with a 60-fold w/w excess of a different unlabeled competing DNA in TAE buffer. These samples were loaded into lanes 6–8 of the gel. For lanes 4 and 5, 1.6×10^{-8} M EthD (final concentration) was mixed with a large amount of either pBluescript dsDNA (final concentration, 1.4×10^{-5} M bp) or M13 ssDNA (final concentration, 2.8×10^{-5} M bases) to serve as controls for the fluorescence intensity expected for 100% transfer of dye to either dsDNA or ssDNA. The type and total amount of DNA loaded into each lane, and the DNA to dye ratio (in bp/dye for dsDNA and bases/dye for ssDNA) in the initial DNA–dye complex are indicated below the gel. For gel image acquisition, see legend to Figure 3.

complex formed between dsDNA and EthD. (The concentration of EthD used in lanes 3 and 8 is greater than that used in the other lanes in order to facilitate the imaging of the weaker M13 ssDNA–EthD fluorescence. As a result, the intensities of the bands in these two lanes can be compared to each other, but should not be directly compared to the fluorescence intensities in the other lanes.) Lanes 6–8 show the various transfer reactions, where the competing DNA was maintained at a constant 60-fold excess (w/w) over the pre-labeled EthD–DNA sample. The results are qualitatively similar to those obtained with the TOTO complexes. The ssDNA–EthD complex retains a substantial amount of dye even when incubated with a 60-fold weight excess of competing dsDNA (lane 8).

DISCUSSION

Extensive work over a number of years has borne out the initial hypothesis (29), that the most stable binding mode of many planar heteroaromatic cations with dsDNA involves the insertion of a conjugated ring system into the interior of the helix, nestled between the adjacent base pairs of the DNA. However, the findings presented here suggest that interactions that presumably do not generally involve 'classical' intercalation can result in dye–ssDNA complexes of remarkably high stability.

The similarities in affinity and spectroscopic properties between the dsDNA– and ssDNA–TOTO complexes suggest that they share at least some structural characteristics in common. However, differences between the two types of complexes include: (a) quantitative differences in the absorbance, circular dichroism, and fluorescence spectra of the two types of complexes at similar dye/DNA ratios (Figs 1 and 2); (b) different direction of electrophoretic mobility shift as a function of binding site saturation (Fig. 3); and (c) differences in the stabilities at high cation concentrations.

At least two simple hypotheses can be offered to explain these results. The first explanation would propose that the strong dye-binding sites on the M13 ssDNA are in self-complementary double-stranded regions (e.g., hairpins) in the mostly single-stranded DNA polymer. Quantitative aspects of the ssDNA–dye interaction argue strongly against this explanation. At 15 bases/dye, virtually all of the added dye is stably associated with the single-stranded polymer as evidenced by the lack of extensive fluorescence in the pBluescript bands from lanes 2 and 3 of Figure 3. This result indicates that in the initial labeling of the ssM13 sample, little or no free TOTO remains in solution. The saturation of TOTO fluorescence with dsDNA at 4–5 bp/dye (Fig. 2A) is consistent with a primary binding site coverage of 4–5 bp for TOTO, similar to the binding site size observed with other very similar bis-intercalating ligands [e.g. EthD; (15,30)]. Therefore, at 15 bases/dye, for all the dye to be bound to double-stranded regions of the ssDNA, two-thirds of the M13 ssDNA molecule would have to be double-stranded. Thermal melting curves of the M13 ssDNA (data not shown) provide no evidence for a significant content of double-stranded regions. These melting curves are broad and show hyperchromic changes similar to those seen in the melting profiles of single-stranded homopolymers. In addition, if the binding sites for TOTO were equivalent in M13 ssDNA and dsDNA, it would be anticipated that the fluorescence properties of the two types of complexes would likewise be the same. However, the data in Figures 2 and 3 demonstrate that at 15 bases/dye (or bp/dye), the fluorescence yield per bound dye is much lower for ssDNA than for dsDNA.

Since binding of TOTO to classical (i.e. Watson–Crick) double-stranded regions of the ssDNA does not appear to be a likely explanation for the observed stable binding of the dye, binding interactions that involve dye stacking need be considered. Cyanine dyes like the thiazole orange head groups of TOTO have a strong tendency to stack in aqueous solution (31), a phenomenon noted above. A dye stacking model was proposed to explain weak binding of a number of cationic dyes to anionic biological polymers (like nucleic acids and negatively charged polypeptides). In this model, the charge interactions between an anionic polymer and cationic dyes promote the formation of stacked dye aggregates along the polymer backbone (32,33). This type of interaction has typically been classified as a 'weak' interaction and is generally disrupted above 100 mM NaCl (30). Such an 'external' stacking model is inconsistent with the high stability of the ssDNA–TOTO complex to high concentrations of cations.

However, other forms of stacking interactions can be envisioned that could explain the behavior of TOTO. Pritchard and colleagues (34) proposed a partial intercalation model of cationic dye binding to DNA as an alternative to the classical intercalation model of Lerman (29), partly as a way to explain the extensive and stable associations of acridine dyes with homopolymers or denatured DNA (28,34–39). This model envisioned the stacking of cationic dyes between two adjacent bases on the same strand of DNA rather than between four bases from two strands, with the

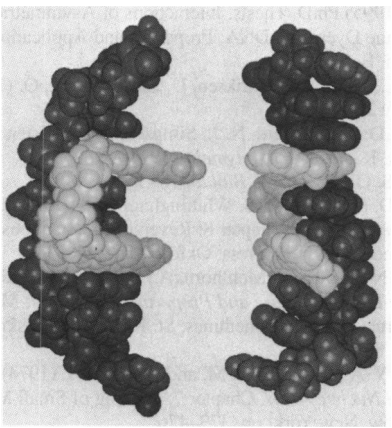

Figure 6. Model of TOTO bound to ssDNA with both thiazole orange head groups partially intercalated between the bases of a single DNA strand. This possible binding mode was extrapolated from the coordinates of an NMR structure for a TOTO–dsDNA complex formed in solution (see text). The DNA strand shown is one strand of the actual NMR structure and the coordinates of this structure have not been altered. The torsion angles of the TOTO backbone and the methine linkage of the thiazole orange head group were slightly modified from the actual structural coordinates in order to obtain a reasonable fit against the DNA strand by visual inspection. The model was built using Insight II (Biosym; San Diego, CA) on an Iris Indigo workstation (Silicon Graphics; Mountain View, CA) and the image was graphically finished using Photoshop (Adobe; Mountain View, CA) on a Macintosh PC (Apple; Cupertino, CA).

dye positive charge aligned for favorable coulombic interactions with the single-strand phosphate. Darzynkiewicz and Kapuscinski extended this model to explain both the stable binding interactions of acridine orange with single-stranded nucleic acids, as well as the apparent capability of this dye to denature dsDNA under certain conditions (40–44). In their model, the single-stranded polymer serves as a scaffold upon which highly cooperative dye–base–dye stack aggregates are formed.

The model that appears to account best for the stability and spectroscopic properties of the TOTO–ssDNA complex is one which invokes a combination of stacking interactions between the thiazole orange head groups of the dimer and the bases of the single-stranded polymer together with coulombic interactions between the positive charges on the dye and the negative charges on the DNA (a 'partial intercalation-like' complex). Stacking of the thiazole orange head groups between the bases of ssDNA would also result in the types of electronic dipole interactions present in dsDNA–TOTO complexes that lead to changes in the absorption spectrum and optical activity of the bound dye. This would account for the general similarities in the properties of the dsDNA- and ssDNA-bound dye. Subtle differences in the exact orientation of the dye chromophores, in the mobility of the bound dye, or in solvent accessibility, could then explain the quantitative difference in the spectroscopic properties, particularly the differences in fluorescence intensity. A possible model for the binding of TOTO to ssDNA that attempts to take into account these various aspects is shown in Figure 6. This model is based upon a solution NMR structure of TOTO bound to an octamer of dsDNA (Jens Peter Jacobsen, David Wemmer and colleagues, personal communication).

The model in Figure 6 shows the TOTO dye bound in the ssDNA-equivalent of a bis-intercalation complex. While competition experiments between ssDNA–TOTO and dsDNA suggest that transfer resistant dimers are bound in this fashion, the flexibility of a ssDNA strand is likely to accommodate a variety of binding modes. The data described here cannot, for example, confirm or eliminate the possibility that TOTO binding to the M13 ssDNA induces the formation base paired or hairpin-like structures that are stabilized only by the association of the dimeric dye. However, such structures could not, based upon the data presented, be classical Watson–Crick base pairs. Binding conformations that involve the stacking of thiazole head groups with each other along the exterior of the ssDNA, stabilized by a limited number of partially intercalated thiazole head groups are similarly likely. This model accounts well for the spectroscopic properties of the TOTO complexes with polydA, polydT and polydC, where blue shifts in the absorption spectrum of the dye when bound to the homopolymers, the very weak fluorescence of the TOTO–homopolymer complexes, and the complicated, multicomponent induced CD spectra of the TOTO–homopolymer complexes all indicate dye–dye interactions (26). The fact that the ssDNA–TOTO complex is more stable to cation-induced dissociation suggests that the polyelectrolyte effects that are so pronounced in the binding of cationic dyes to dsDNA contribute less to the binding free energy of TOTO–ssDNA complexes.

The observations on the ssDNA–TOTO complex appear to hold for ssDNA interactions with the structurally unrelated homodimeric dye, EthD (Fig. 5), and thus appear to be generally relevant to the understanding of the interaction of ssDNA with other polycationic dimeric dyes capable of intercalation. The unexpected stability of the ssDNA–dye complexes can most likely be exploited in the applications already described for fluorescent dsDNA–dye complexes (1).

Finally, on a cautionary note, the tendency of the bound dye to transfer from a stable DNA complex to binding sites on unlabeled nucleic acid molecules upon an increase in cation concentration must be considered when dyes such as TOTO are employed as cytological stains or specific nucleic acid labels under various conditions.

ACKNOWLEDGEMENTS

We thank Scott C. Benson for providing us with dyes, and Drs David Wemmer and Jens Peter Jacobsen for sharing the coordinates of a dsDNA–TOTO complex prior to publication. We are grateful to Richard A. Mathies for advice and helpful discussions throughout the course of this work. This research was supported in part by a grant from the Director, Office of Energy Research, Office of Health and Environmental Research of the US Department of Energy under contract DE-FG-91ER61125.

REFERENCES

1 Glazer, A. N. and Rye, H. S. (1992) *Nature* **359**, 859–861.
2 Benson, S. C., Mathies, R. A. and Glazer, A. N. (1993) *Nucleic Acids Res.* **21**, 5720–5726.
3 Rye, H. S., Yue, S., Quesada, M. A., Haugland, R. P., Mathies, R. A. and Glazer, A. N. (1993) *Methods Enzymol.* **217**, 414–431.
4 Rye, H. S., Yue, S., Wemmer, D. E., Quesada, M. A., Haugland, R. P., Mathies, R. A. and Glazer, A. N. (1992) *Nucleic Acids Res.* **20**, 2803–2812.
5 Zhu, H., Clark, S. M., Benson, S. C., Rye, H. S., Glazer, A. N. and Mathies, R. A. (1994) *Anal. Chem.* **66**, 1941–1948.
6 Rye, H. S., Drees, B. L., Nelson, H. C. M. and Glazer, A. N. (1993) *J. Biol. Chem.* **268**, 25229–25238.

7 Rye, H. S., Dabora, J. M., Quesada, M. A., Mathies, R. A. and Glazer, A. N. (1993) *Anal. Biochem.* **208**, 144–150.
8 Castro, A., Fairfield, F. R. and Shera, E. B. (1993) *Anal. Chem.* **65**, 849–852.
9 Goodwin, P. M., Johnson, M. E., Martin, J. C., Ambrose, W. P., Marrone, B. L., Jett, J. H. and Keller, R. A. (1993) *Nucleic Acids Res.* **21**, 803–806.
10 Hirons, G. T., Fawcett, J. J. and Crissman, H. A. (1994) *Cytometry* **15**, 129–140.
11 Srinivasan, K., Morris, S. C., Girard, J. E., Kline, M. C. and Reeder, D. J. (1993) *Applied and Theoretical Electrophoresis* **3**, 235–239.
12 Auzanneau, I., Barreau, C. and Salome, L. (1993) *Compt. Rend. de l'Acad. Sci. Serie III, Sciences de la Vie* **316**, 459–462.
13 Perkins, T. T., Smith, D. E. and Chu, S. (1994) *Science* **264**, 819–822.
14 Perkins, T. T., Smith, D. E. and Chu, S. (1994) *Science* **264**, 822–826.
15 Gaugain, B., Barbet, J., Capelle, N., Roques, B. P. and Le Pecq, J. B. (1978) *Biochemistry* **17**, 5078–5088.
16 Gaugain, B., Barbet, J., Oberlin, R., Roques, B. P. and Le Pecq, J. B. (1978) *Biochemistry* **17**, 5071–5078.
17 Glazer, A. N., Peck, K. and Mathies, R. A. (1990) *Proc. Natl. Acad. Sci. USA* **87**, 3851–3855.
18 Markovits, J., Roques, B. P. and LePecq, J. B. (1979) *Anal. Biochem.* **94**, 259–264.
19 Fujiwara, T., Giesman-Cookmeyer, D., Ding, B., Lommel, S. A. and Lucas, W. J. (1993) *The Plant Cell* **5**, 1783–1794.
20 Noueiry, A. O., Lucas, W. J. and Gilbertson, R. L. (1994) *Cell* **76**, 925–932.
21 Haugland, R. P. (1992) Molecular Probes: Handbook of Fluorescent Probes and Research Chemicals. pp. 221–228, Molecular Probes, Inc., Eugene, OR.
22 Ausubel, F. M., Brent, R., Kington, R. E., Moore, D. D., Seidman, J. G., Smith, J. A. and Struhl, K. (ed.) (1992) Short Protocols in Molecular Biology, 2nd. Greene Publishing Associates and John Wiley & Sons, New York, NY.
23 Rye, H. S., Quesada, M. A., Peck, K., Mathies, R. A. and Glazer, A. N. (1991) *Nucleic Acids Res.* **19**, 327–333.
24 Mathies, R. M., Scherer, J. R., Quesada, M. A., Rye, H. S. and Glazer, A. N. (1994) *Rev. Sci. Instrum.* **65**, 807–812.
25 Quesada, M. A., Rye, H. S., Gingrich, J. C., Glazer, A. N. and Mathies, R. A. (1991) *BioTechniques* **10**, 616–625.
26 Rye, H. S. (1995) Ph.D. Thesis, Interactions of Asymmetric Cyanine and Phenanthridine Dyes with DNA: Properties and Applications, University of California, Berkeley.
27 Nielsen, P. E., Zhen, W., Henriksen, U. and Buchardt, O. (1988) *Biochemistry* **27**, 67–73.
28 Drummond, D. S., Pritchard, N. J., Simpson-Gildemeister, V. F. W. and Peacocke, A. R. (1966) *Biopolymers* **4**, 971–987.
29 Lerman, L. S. (1961) *J. Mol. Biol.* **3**, 18–30.
30 Wilson, W. D. (1990) In M. S. Whittingham and A J. Jacobsen (ed), *Intercalation Chemistry.* Chapter 8: Reversible interactions of nucleic acids with small molecules, IRL Press, Oxford, pp. 297–336.
31 Tyutyulkov, N., Fabian, J., Mehlhorn, A., Dietz, F. and Tadjer, A. (1991) *Polymethine Dyes. Structure and Properties.* Chapter V: Molecular and aggregate structures of polymethines, St. Kliment Ohridski University Press, Sofia, 89–121.
32 Bloomfield, V. A., Crothers, D. M. and Tinoco, I. J. (1974) *Physical Chemistry of Nucleic Acids.* Chapter 7: Binding of Small Molecules, Harper & Row, New York, pp. 373–476.
33 Bradley, D. F. and Wolf, M. K. (1959) *Proc. Natl. Acad. Sci. USA* **45**, 944–952.
34 Pritchard, N. J., Blake, A. and Peacocke, A. R. (1966) *Nature* **212**, 1360–1361.
35 Blake, A. and Peacocke, A. R. (1966) *Biopolymers* **4**, 1091–1104.
36 Blake, A. and Peacocke, A. R. (1967) *Biopolymers* **5**, 383–397.
37 Blake, A. and Peacocke, A. R. (1968) *Biopolymers* **6**, 1225–1253.
38 Dourlent, M. and Helene, C. (1971) *Eur. J. Biochem.* **23**, 86–95.
39 von Tscharner, V. and Schwarz, G. (1979) *Biophys. Struct. Mechanism* **5**, 75–90.
40 Darzynkiewicz, Z. and Kapuscinski, J. (1990) In M. R. Melamed, L. Tore and M. L. Mendelsohn (ed.), *Flow Cytometry and Sorting.* Acridine orange: A versatile probe of nucleic acids and other cell constituents, 2nd ed. Wiley-Liss, New York, 291–314.
41 Kapuscinski, J. and Darzynkiewicz, Z. (1983) *Nucleic Acids Res.* **11**, 7555–7568.
42 Kapuscinski, J. and Darzynkiewicz, Z. (1984) *J. Biomol. Struct. Dyn.* **1**, 1485–1499.
43 Kapuscinski, J. and Darzynkiewicz, Z. (1987) *J. Biomol. Struct. Dyn.* **5**, 127–143.
44 Kapuscinski, J., Darzynkiewicz, Z. and Melamed, M. R. (1983) *Biochem. Pharmacol.* **32**, 3679–3694.